Proceedings of the ASME 2021
Fluids Engineering Division Summer Meeting
FEDSM2021
August 10-12, 2021, Virtual, Online

FEDSM2021-65637

A HYBRID HIGH-ORDER VORTICITY-BASED EULERIAN AND LAGRANGIAN VORTEX PARTICLE METHOD, THE 2-D CASE

Mark J. Stock
Applied Scientific Research, Inc.
Irvine, California
Email: markjstock@gmail.com

Adrin Gharakhani
Applied Scientific Research, Inc.
Irvine, California
adrin@applied-scientific.com

ABSTRACT

Hybrid Lagrangian-Eulerian solvers combine the convective and compactness advantages of vortex methods with the spatial anisotropy and boundary-resolving advantages of Eulerian methods to create flexible solvers capable of adequately capturing thin boundary layers while still maintaining wake vortex coherency for unsteady incompressible flow in complex geometries. The present paper details a new hybrid method which combines, in one open-source package, a novel, compact, high-order Eulerian scheme for vorticity transport to predict the flow in the near-boundary region with a grid-free, unremeshed, Lagrangian Vortex Particle Method (LVPM) for the off-boundary vorticity-containing region. This paper focuses on the hybridization of the two methods and demonstrates its effectiveness on two canonical benchmarks: flow in 2-D lid-driven cavity at Re = 1,000 *and impulsively started flow over a circular cylinder at* Re = 9,500*. In each case, the hybrid method improves upon a pure LVPM and uses far fewer cells than a purely Eulerian scheme. In addition, the size of the associated Eulerian region is greatly reduced compared to previous hybrid methods.*

NOMENCLATURE

d_{wall}	Distance from a point to the nearest wall boundary.
d_{open}	Distance from a point to the nearest open boundary.
$\hat{d}$	Non-dimensionalized distance of a point from a wall to an open boundary.
D	Diameter.
h	Cell size.
N_c	Number of cells/elements.
N_p	Number of panels.
N_v	Number of vortex particles.
R	Radius.
Re	Reynolds number.
t	Time.
t_R	Time non-dimensionalized by radius.
$\boldsymbol{n}$	Surface normal vector.
$\boldsymbol{u}$	Velocity vector.
$\boldsymbol{U}_\infty$	Freestream velocity vector.
$\boldsymbol{x}$	Position vector.
Γ	Circulation ($\omega\, dA$ in 2-D).
Δt	Computational time step.
Δx	Cell size or interparticle spacing.
σ	Core radius of particle smoothing function.
$\phi_{g\to p}$	Grid-to-particle scalar field.
$\phi_{p\to g}$	Particle-to-grid scalar field.
$\boldsymbol{\omega}$	Vorticity vector.

INTRODUCTION

Lagrangian Vortex Particle Methods (LVPM) are well-suited for simulation of unsteady vortex-dominated incompressible fluid flow in the moderate Reynolds number regime, including transitional flow. Key advantages of LVPM are (1) near absence of numerical diffusion, thanks to the Lagrangian accounting of convection; (2) dynamic solution adaptivity resulting from the inherent ability of vortex elements to automatically convect toward regions with high vorticity strength; and (3) excellent ca-

pacity for high-efficiency parallelization and vectorization due to the high arithmetic intensity of the Biot-Savart formulation. However, accurate and efficient treatment of the flow near the boundary, which invariably requires the use of anisotropic vortex elements, has remained mostly elusive to date. On the other hand, compact high-order Eulerian CFD methods have recently demonstrated excellent accuracy and computational efficiency on canonical problems; however, they are rather challenging to apply to problems that involve multiple bodies in relative motion, such as those observed in many cardiovascular devices; and also have not been extended to use velocity-vorticity variables.

To this end, leveraging the best attributes of these two very diverse approaches, we demonstrate a new open-source hybrid CFD solver, which combines a vorticity-based high-order Eulerian method for accurate prediction of the near-body flow with a LVPM for off-body CFD to solve unsteady incompressible flow in complex geometries. This paper focuses on the hybridization of the Eulerian and Lagrangian solutions in a smooth and accurate manner. An accompanying paper discusses the Eulerian solution in more detail [1].

The earliest attempts at merging an Eulerian solver for the boundary layer with an LVPM for the wake used non-overlapping regions [2, 3]. Subsequent hybrid solvers [4, 5] introduced the concept of using domain decomposition with overlapping to ease the burden of matching flow properties at the interface. These depended, though, on a costly iterative Schwarz method to refine the solution of the boundary conditions. Daeninck [6] laid out a hybrid method which removed this requirement and became the basis for many subsequent techniques. In their method, a 2nd order velocity-vorticity solver resolves the near-wall region, and the vorticity in the Eulerian region is interpolated onto particles. It was applied to several two-dimensional flows. A number of coincident papers [7–9] follow the previous work into three dimensions with minor differences. Because of their application to problems in rotary-wing aerodynamics, many incorporate a velocity-pressure Eulerian method, and the thickness of the Eulerian regions are typically on the order of a chord length. Oxley [10] and then Papadakis & Voutsinas [11] address compressibility using a Lagrangian method which tracks dilatation, though these still require a relatively large Eulerian region. Palha *et al.* [12] provides a thorough overview of this history, and a hybrid method that, like previous authors, updates the Lagrangian particle circulations on an intermediate regular grid.

In the proposed method, the computational domain for the Eulerian solver covers only a layer above any wall boundaries, and ends in an open boundary to the Lagrangian regime. Lagrangian vortex particles exist within this domain and in the wake. In one single outer time step, the LVPM marches ahead to provide the velocity and vorticity boundary conditions on the open boundary of the high-order mesh. The high-order Eulerian solver then simulates that same outer time step over a larger number of inner time steps, each involving solutions of convection, diffusion, and a Poisson solution for the vorticity-velocity inversion. At the end of those substeps, the vorticity in the Eulerian domain is used to reset strengths on any co-located vortex particles. The vortex particles then help reset any discontinuities in the vorticity in the outer reaches of the Eulerian domain. In this manner, vorticity is able to smoothly exit and enter the Eulerian domain while still far more accurately modeling the high gradients expected near the wall.

To study the performance and accuracy of the proposed method, we simulated several canonical viscous flow problems such as the 2-D lid-driven cavity at Re = 1,000 and an impulsively started circular cylinder at Re = 9,500. The new method is shown to be able to resolve near-wall regions that would have required a far-more computationally-intense purely Lagrangian solution, ensuring long-term accuracy of viscous vortical flows.

This paper details the first known hybridization of a high-order Eulerian scheme for resolution of near-body regions with a Lagrangian Vortex Particle Method for off-body regions. This, combined with a new method to update strengths of the Lagrangian particles from the Eulerian solution, allows hybrid simulations to remain accurate with significantly smaller Eulerian regions compared to previous work.

HYBRID METHOD

The software uses a desingularized LVPM to discretize the vorticity and an augmented Boundary Element Method (BEM) to enforce boundary conditions. These methods are summarized below, but extensive background [4, 13] and implementation-specific details [14, 15] can be found elsewhere.

Lagrangian Vortex Particle Method

The governing equations of incompressible fluid flow in terms of the transport of vorticity are

$$\frac{\partial \boldsymbol{\omega}}{\partial t} + \boldsymbol{u}\cdot\nabla\boldsymbol{\omega} = \boldsymbol{\omega}\cdot\nabla\boldsymbol{u} + \frac{1}{\mathrm{Re}}\nabla^2\boldsymbol{\omega} \tag{1}$$

$$\nabla\cdot\boldsymbol{u} = 0 \tag{2}$$

$$\nabla\times\boldsymbol{u} = \boldsymbol{\omega} \tag{3}$$

supplemented with the appropriate velocity and vorticity boundary conditions. In two dimensions, vorticity is a scalar and the stretching term is identically zero. Specific details of the methods and algorithms used presently appear in our previous work [16].

In the LVPM, the vorticity field is discretized using N_v smooth vortex particles, each with constant core radius σ and circulation Γ_i. Viscous diffusion is evaluated using the Vorticity Redistribution Method (VRM) [17, 18]. VRM works by redistributing the circulation Γ_i of each diffusing particle to neighboring particles such that the moments of the diffusion equation

are conserved up to arbitrary order, with new particles created *only* if required to satisfy the moment equations. In this work we conserve up to and including the 2nd moment. Additionally, in order to prevent unbounded growth of N_v, VRM is applied only to particles with circulation greater than a dynamic threshold, in this case $|\Gamma_i| > 10^{-5}\,|\Gamma|_{\max}$. Note that VRM allows the present method to avoid any ad-hoc regridding that is common in most other vortex methods.

Velocities are computed from the integration of the Biot-Savart equation over the entire vorticity-containing region. A Boundary Element Method serves to enforce boundary condition at walls, and unlike most other hybrid methods, explicitly generates vorticity on the fluid side of the boundary. Convection is integrated using a second-order Runge-Kutta method. The convection and diffusion functions operate within a 2nd order operator-splitting scheme, in which one half step of diffusion is followed by a full convection step and then another half step of diffusion.

Eulerian High-Order Solver

Grids are created on solid boundaries and extend a limited distance into the flow. A high-order, vorticity-based Eulerian solver governs the flow in this regime. Vorticity transport in this near-body subdomain is discretized via a newly developed compact, high-order, discontinuous spectral difference method based on the flux reconstruction method of Huynh [19, 20]. Details of this new method are beyond the scope of this paper and are presented in an accompanying work [1]. The geometric meshes are generated using *gmsh* [21], and from those high-order quadrilateral elements the solution nodes are placed at Gauss-Lobatto points in each dimension.

Each time step is advanced with a Runge-Kutta method (2nd to 4th order), and each substep of those methods performs the following operations.

1. Solve a *Poisson problem* for streamfunction and use the gradients to determine the velocity. Wall boundaries use a constant-valued Dirichlet boundary condition, and open boundaries use the tangential velocity as a Neumann boundary condition.
2. Compute *velocity jump* at the solid boundaries from the above.
3. Compute *diffused flux*. Wall boundaries use a Neumann boundary condition for vorticity to render the velocity jumps null [1, 22], and open boundaries use vorticity as a Dirichlet boundary condition.
4. Compute *convected flux*. All boundaries use vorticity times the normal velocity as a Dirichlet boundary condition.

Hybridization

The Eulerian and Lagrangian regions are connected in a manner similar to previous methods designed to avoid expensive implicit iterations [6,7,12]. A Lagrangian Vortex Particle Method solves for the flow properties in the entire fluid domain, from the wall to infinity, while an Eulerian solver is only used for near-body regions, and acts to correct the Lagrangian solution near the body. As the Eulerian regime generally contains the largest vorticity values and gradients, it operates with higher spatial resolution and smaller time steps than the outer Lagrangian regime, primarily dictated by convective and diffusive criteria for computational stability. Thus, each Lagrangian (outer) time step generally requires several Eulerian (inner) time steps.

The Lagrangian region affects the Eulerian region via two mechanisms: setting boundary conditions on the Eulerian regions' open boundaries, and adjusting the vorticity in the outer reaches of the Eulerian region. The latter is the particle-to-grid feedback zone, defined by a constant scalar field $\phi_{p\to g}$ evaluated on every solution node in the Eulerian region at the beginning of the calculation.

The Eulerian region affects the Lagrangian region via one mechanism, acting at the end of each outer time step: adjusting particle circulations within a band called the grid-to-particle feedback zone (or "Lagrangian adjustment region"). This zone is defined by a constant scalar field $\phi_{g\to p}$ evaluated at every solution node in the Eulerian region at the beginning of the calculation.

In all simulations presented herein, these scalar fields are defined with the following functions of the normalized distance of the solution node from the body to the open boundary ($\hat{d}$), though other functions may be similarly effective.

$$\hat{d} = \frac{d_{wall}}{d_{wall} + d_{open}} \tag{4}$$

$$\phi_{p\to g} = \begin{cases} \cos^2(2\pi\hat{d}) & \text{if } \hat{d} > 0.75 \\ 0 & \text{otherwise} \end{cases} \tag{5}$$

$$\phi_{g\to p} = \begin{cases} \cos^2(2\pi\hat{d}) & \text{if } 0.25 < \hat{d} < 0.75 \\ 0 & \text{otherwise} \end{cases} \tag{6}$$

While Daeninck [6] allows adjustment of particle strengths down to the wall, we experienced difficulties interpolating the rather strong vorticity values present very close to the wall, and thus our "Lagrangian adjustment region" operates on the middle of the Eulerian region, similar to Palha *et al.* [12] and our previous work [7]. A final note here is that the present method uses a Boundary Element Method, and not the Eulerian region, to satisfy the wall boundary conditions for the Lagrangian solver.

An outline of the hybrid method, which follows Daeninck [6], Stock & Gharakhani [7], and Palha *et al.* [12], appears below.

1. At time t the solution is known in both the Eulerian and Lagrangian regimes, though it is assumed that the Lagrangian solution is less accurate near the wall.
2. The complete Lagrangian system advances one full (outer) time step.
3. A set of data is passed from the Lagrangian to the Eulerian solver, containing:
   - Velocity and vorticity on the open boundary nodes of the Eulerian regime at the beginning and ending of the outer time step, as calculated by the Lagrangian solver;
   - Vorticity and particle-to-grid weights at all solution nodes of the Eulerian regime at the beginning and ending of the outer time step, as calculated by the Lagrangian solver.
4. The Eulerian solver advances a number of (inner) time steps, each time step involving:
   (a) Setting the open boundary conditions using velocities and vorticities from the Lagrangian solution, linearly interpolated in time for the given step and integrator sub-step;
   (b) Performing the Runge-Kutta integration to advance the Eulerian vorticity transport equations; and
   (c) Using the particle-to-grid weights and the Lagrangian vorticity, linearly interpolated in time, to nudge the vorticity in the Eulerian regime near the open boundary.
5. In the grid-to-particle overlap region, the vorticity from the Eulerian solution is transmitted to the Lagrangian solution in a manner similar to Beale [23]. This consists of the following steps:
   (a) The vorticity deficit is calculated on each Eulerian solution node using vorticity from each of the two regimes;
   (b) This is then scaled by the area of the solution node and then again by the weight from the grid-to-particle field;
   (c) New Lagrangian particles are created at the centers of the solution nodes, using this scaled circulation, only if that circulation is above a threshold;
   (d) These particles are merged with the underlying Lagrangian vortex particles;
   (e) The vorticity on the Eulerian solution nodes is then recalculated from the Lagrangian vortex particles, and a new vorticity deficit is calculated; and
   (f) The above process is repeated up to 10 times, or until the relative magnitude of the vorticity deficit is below 10^{-4}.
6. The solution at $t + \Delta t$ is now current in both the Eulerian and Lagrangian regimes.

The grid-to-particle update (step 5 above) is the main difference between the present and previous hybrid methods. The implementation used herein is relatively costly but can be improved with a least-squares matrix solution for the circulation change required to best match the Eulerian vorticity. This is a goal of subsequent research.

Implementation

The open-source *Omega2D* [16, 24] solver was used as the driver for the present method. This is an open-source, cross-platform, C++11/14/17 program with a graphical user interface, and in this work it performed the Lagrangian (particle) simulation and hybridization portions of the solution, but not the Eulerian solution. All Biot-Savart summations in this program use the Vatistas $n = 2$ core function [25] and direct $O(N^2)$ summations, though algorithms with lower order of operations exist [26, 27] and may be implemented in the future. Nevertheless, extensive performance optimization using multithreading and explicit vectorization allow simulations to run at interactive rates.

The driver program can link to any Eulerian solver which exposes the appropriate calls, which itself can use one of a variety of matrix solvers. All results herein used a Fortran 90 Eulerian solver developed under the same grant, though a C++ solver is expected to be integrated into the package. Additionally, matrix solutions were performed by a proprietary multi-threaded solver called APLLES, though AMGCL [28] is also effective.

All tests below were performed on an 8-core Intel i7-5960X running Fedora Linux.

VALIDATION

Two canonical flows were created and run with our open-source *Omega2D* LVPM solver: a lid-driven cavity and flow over an impulsively-started circular cylinder. In each case, the results compare favorably with prior art.

Lid Driven Cavity in 2-D

A canonical test of internal flow is the lid driven cavity, which has well-known solutions at many Reynolds numbers. In this flow, a closed, unit square box with fluid initially at rest is driven by tangential motion of the top lid at unit speed to the right. Previous results from Ghia *et al.* [29] for the steady-state Re = 1,000 case were performed with a uniform 129×129 point finite difference grid and solved with multigrid relaxation. Subsequently, Erturk *et al.* [30] refined those results for a wide range of high Reynolds numbers, using 601×601 points on the finest grid and performing Richardson extrapolation to estimate the solutions.

Simulations were made at multiple resolutions ($\Delta t_{part} = 0.04, 0.01, 0.0025$), with both pure Lagrangian and hybrid Lagrangian-Eulerian methods, with the Eulerian regions composed of only 3rd-order square elements extending $0.1L$ from the walls. Note that for the lowest-resolution case, this resulted in a layer only three cells thick. Nominal particle separation was set to $\Delta x_{part} = \sqrt{6\Delta t_{part}/\mathrm{Re}}$, and overlap ratio was 2. All simulations

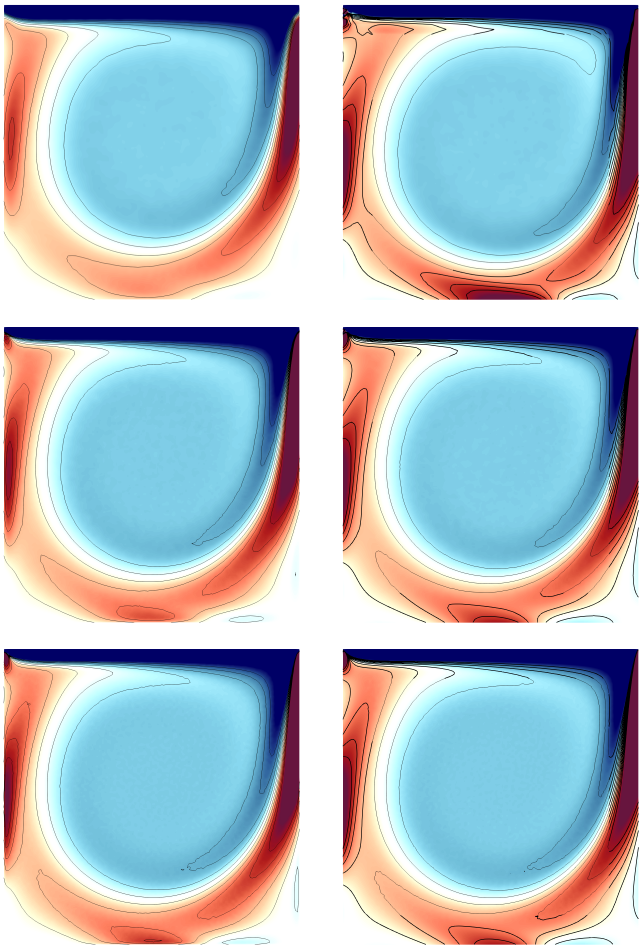

FIGURE 1. 2-D DRIVEN CAVITY, RE=1,000, VORTICITY AT T = 75, CONTOURS AT $\pm\{0.5,1.5,2.5,3.5,4.5\}$; LEFT: PARTICLE ONLY, RIGHT: HYBRID, TOP TO BOTTOM: $\Delta T_P = \{0.04,0.01,0.0025\}$.

used VRM diffusion with a relative particle strength threshold of 10^{-5}.

Figure 1 shows the vorticity fields for several of these runs. Clear from this figure is that the particle-only runs underestimate vorticity at the wall, while the lowest resolution hybrid case overestimates it (likely due to the very thin and active grid-to-particle overlap region). Table 1 shows runtime parameters and selected results for our hybrid simulations and those of Erturk *et al.* [30]. Because of the relationship in the present method between Δt and Δx, the number of particles increases by four-fold as the time step is reduced by a similar factor. As the present method is intrinsically dynamic, each simulation was run to $t = 75$, though the flow continued to evolve, albeit subtly, afterward. We estimate the error due to stopping the simulations early to be roughly $\approx 0.1\%$. As resolution increases, the results converge to the solution from Erturk *et al.* [30] at roughly 2nd order. Finally, Figure 2 contains plots of the velocities along centerlines through the cavity. The results for the two highest resolution cases appear to overlap with the results of Ghia *et al.* [29], which at this scale are indistinguishable from Erturk *et al.* [30].

TABLE 1. PARAMETERS AND RESULTS FOR LID DRIVEN CAVITY SIMULATIONS AT THREE RESOLUTIONS.

Parameter	Erturk *et al.*	Present Method		
Δt_{grid}	∞	0.004	0.001	0.00025
Δx_{grid}	$0.001\bar{6}$	$0.0\bar{3}$	0.02	0.01
N_{grid}	361,201	324	900	3,600
Δt_{part}	-	0.04	0.01	0.0025
Δx_{part}	-	0.01549	0.00775	0.00387
$u_{x,y=0.18}$	-0.3869	-0.3659	-0.3792	-0.3847
$u_{x,y=0.94}$	0.4276	0.3901	0.4177	0.4251
$u_{y,x=0.15}$	0.3756	0.3676	0.3665	0.3732
$u_{y,x=0.91}$	-0.5263	-0.5216	-0.5169	-0.5241

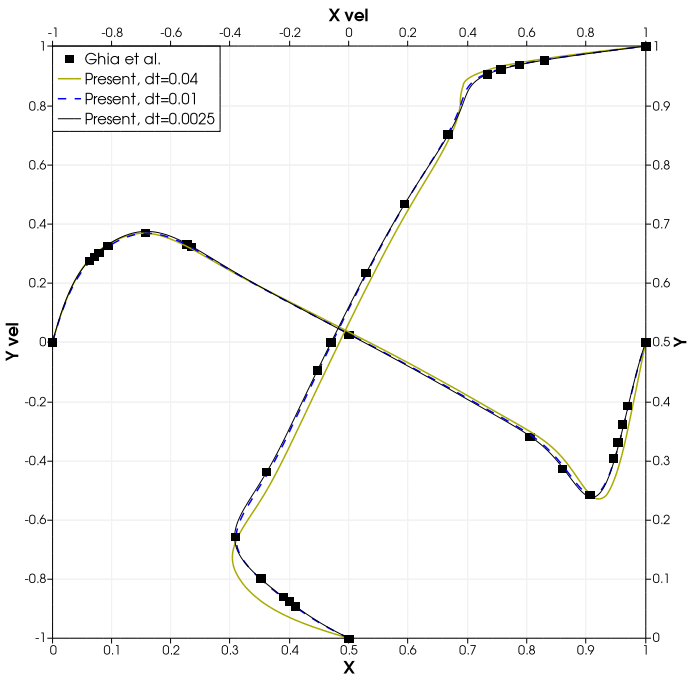

FIGURE 2. 2-D DRIVEN CAVITY, RE=1,000, VERTICAL VELOCITY ALONG HORIZONTAL CENTERLINE, HORIZONTAL VELOCITY ALONG VERTICAL CENTERLINE.

Impulsively Started Cylinder

Impulsively started flow over a circular cylinder is a well-studied problem in two-dimensional fluid dynamics. At intermediate Reynolds numbers, capturing the vorticity field correctly requires careful accounting of the vorticity creation at the boundary, something that has been a challenge for traditional LVPMs. Below we will demonstrate this canonical flow with $\mathrm{Re}_D = 9{,}500$, study the influence of important parameters, and compare our results with previous computations [31–35].

Many computations were performed with purely LVPMs, with Koumoutsakos & Leonard [31] using a particle-strength exchange scheme for diffusion, Shankar [32] the same VRM as the present work, and Wang [34] a diffusion-velocity approach. In a recent implementation of the vortex penalization method [35], diffusion was accomplished with finite differences on a high-resolution regular grid. The final comparison is with a spectral element method solution by Kruse [33], results of which were gathered from Shankar [32]. Other notable studies of this case [36, 37] did not present vorticity fields at the same time steps as the above.

The cases presented below use $D = 1$, $U_\infty = 1$, and $\mathrm{Re}_D = 9{,}500$, Nominal particle separation was set to $\Delta x = \sqrt{6\Delta t_D/\mathrm{Re}}$, overlap ratio was 2, and the cutoff for VRM diffusion was a particle strength magnitude of 10^{-5} relative to the strongest particle. The Eulerian grids consisted of 3rd-order geometric elements, each turned into a 3rd-order computational element by the high-order solver. Following previous authors, time reported in the figures is non-dimensionalized based on the cylinder radius, and most results will be reported at $t_R = 3$ ($t_D = 1.5$ if non-dimensionalized by diameter). Vorticity fields appearing in the following figures contain the complete Eulerian region (up to and including the outer-most row of elements). Outside of the Eulerian region the vorticity is the Lagrangian solution after projecting to an annular grid of 80×500 2nd-order quadrilateral elements in the range $1 \le r/R \le 1.6$. The plots are made in ParaView with the "Cool to Warm (Extended)" palette and a vorticity range of ± 80.

Figure 3 shows our results next to those of the above references. This specific run used $\Delta t_R = 0.0025$, 12 Eulerian substeps, and an Eulerian region extending only to $r/R = 1.05$. Details in the vorticity field downstream of the separation point are difficult to discern from the older references, but all four methods seem to capture the position and sizes of the secondary parcels of vorticity. The most notable difference is in the thin region of positive vorticity (red) immediately adjacent to the first primary shed vortex (blue), the magnitude of which is not reported in the literature, though the position is readily comparable. On this criterion, the present results more closely resemble the earlier VRM calculations than the spectral method. A second valuable comparison is the shape of the first primary vortex (blue), which seems more circular in the spectral results, but appears more oval-like in the others.

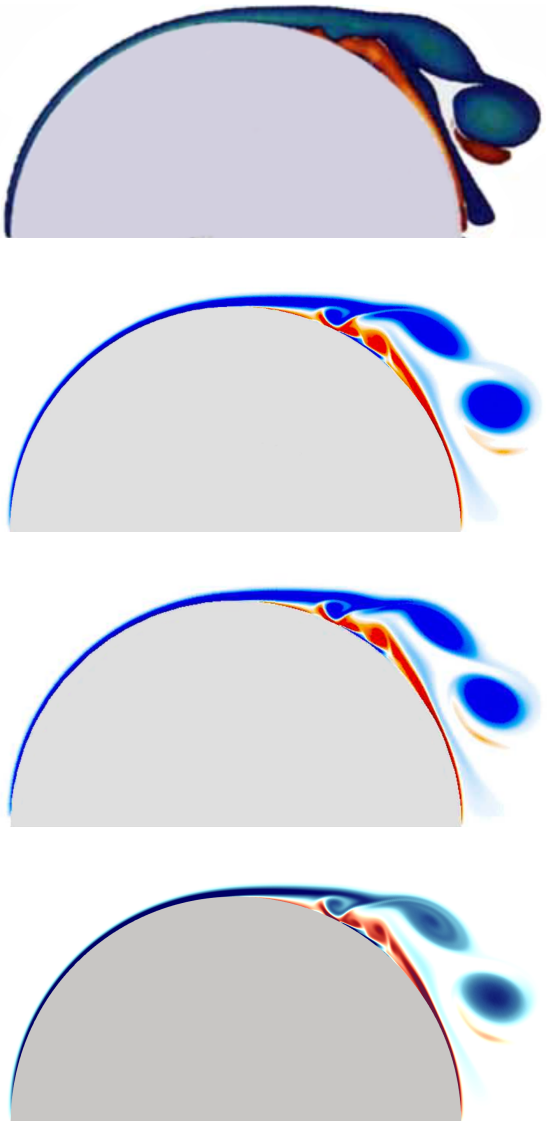

FIGURE 3. 2-D FLOW OVER IMPULSIVELY STARTED CYLINDER, $\mathrm{RE}_D = 9{,}500$, $T_R = 3$, FROM REFERENCES [31], [33], [32], AND PRESENT METHOD (TOP TO BOTTOM).

Effect of element order To determine the influence of Eulerian element order on the solution, we generated four different annular meshes of 3rd-order quadrilateral elements (four nodes on each edge) with *gmsh* such that simulations with 2nd- to 4th-order solution elements would have an equal number of degrees of freedom (41,472). The meshes extended $R \le r \le 1.1\,R$ and contained roughly square quadrilateral elements. Each simulation was run to $t_R = 3$ for purposes of plotting, and to $t_R = 2$ for timing.

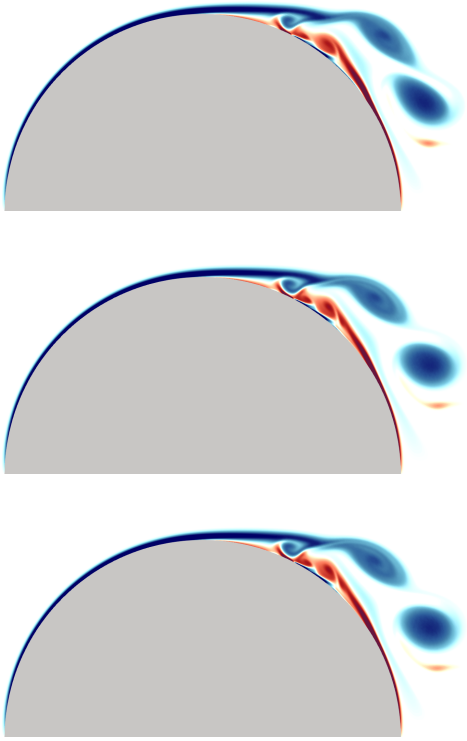

FIGURE 4. 2-D FLOW OVER IMPULSIVELY STARTED CYLINDER, $\mathrm{RE}_D = 9{,}500$, $T_R = 3$, $\Delta T_R = 0.01$, EULERIAN MESH TO $1.1R$, ELEMENT ORDERS 2, 3, 4 (TOP TO BOTTOM).

Vorticity fields from these simulations appear in Fig. 4 and the corresponding parameters in Table 2. Of particular note is that the thickness of the innermost computational elements for the 4th-order case have $h = 0.008$, which is approximately the boundary layer thickness. Visually, the positions and shapes of the two primary negative vortices (blue) constitute the primary difference between the results of orders 2 and 3. Only extremely subtle differences exist when the order of the Eulerian elements is increased to 4. The performance data in Table 2 reveal that the convergence provided by the higher-order meshes come with little additional computational cost. Note that the case with 1st order elements is not presented here, as it was wildly inaccurate.

Effect of size of Eulerian region Clearly, if a hybrid method requires very thick regions above each wall for accuracy, it would amount to little more than a novel boundary condition for the underlying Eulerian solver. Thus, we studied the influence of the size of the Eulerian solution domain on the results, solving the above problem with four different meshes with $1 \leq r/R \leq \{1.05, 1.1, 1.2, 1.5\}$ each with average cell sizes of 0.004, 780 cells around the circumference, and $\{7, 12, 23, 49\}$ cells radially. The Lagrangian particle regime used $\Delta t_R = 0.005$, and the Eulerian regime used 3rd-order solution elements and twelve 4th-order Runge-Kutta substeps per outer time step.

TABLE 2. PARAMETERS AND RESULTS FOR IMPULSIVELY-STARTED CYLINDER SIMULATIONS.

Grid Order	No Grid	2	3	4
Grid Δt_R	-	0.001	0.001	0.001
Grid Δx	-	≈0.004	≈0.006	≈0.008
Grid cells	-	12×864	8×576	6×432
Particle Δt_R	0.01	0.01	0.01	0.01
Particle Δx	0.00178	0.00178	0.00178	0.00178
N_p at $t_R = 3$	153,894	146,786	150,773	151,770
Time to $t_R = 2$	20:05	63:58	66:41	74:05

Vorticity fields of the upper half for these cases appears in Fig. 5. The method has no problem maintaing smooth vorticity across the outer boundary of the Eulerian grid (marked as a thin black line). Similar to the above cases, we see subtle differences in the position and shape of the thin wisp of positive vorticity (red) just below the first primary negative vortex (blue). In the case with the widest Eulerian region, this small patch is thinner and elongated and shifted closer to the body, reminiscent of the Shankar [32] results from Fig. 3, and of the results below with higher particle resolution. A final note is that, even though all cases finished with roughly the same number of vortex particles (about 294,000), the cases with larger mesh volumes, and thus more elements, required commensurately greater wall-clock times to complete.

Very few other differences appear in these results, leading us to conclude that slim body-fitted meshes can accomodate accurate solutions, so long as both regions are fully resolved. Comparatively, no other author has demonstrated Eulerian regions this thin. Cottet & Koumoutsakos [4] used $2R$ for a $\mathrm{Re}_D = 550$ cylinder, and Palha *et al.* [12] used $1.5R$ for the same. Daeninck [6] uses about $1.55R$ for a $\mathrm{Re}_D = 3{,}000$ cylinder.

Effect of particle resolution While the above test cases using the proposed hybrid method involved Eulerian solution node separation distances similar to the nominal particle separation in the LVPM, because much of the evolution of the wake occurs in the purely-Lagrangian regime, we now examine the effect of particle resolution on the results.

Time steps for the four Lagrangian particle resolutions tested are $\Delta t_R = \{0.02, 0.01, 0.005, 0.0025\}$, cor-

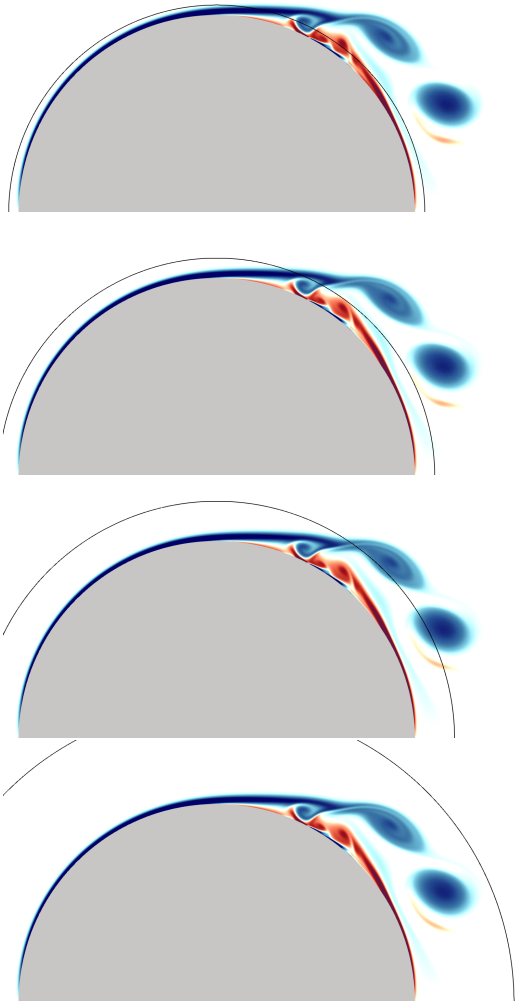

FIGURE 5. 2-D FLOW OVER IMPULSIVELY STARTED CYLINDER, $\mathrm{RE}_D = 9{,}500$, $T_R = 3$, $\Delta T_R = 0.005$, EULERIAN MESH OUTER EXTENTS 1.05 R, 1.1 R, 1.2 R, 1.5 R (TOP TO BOTTOM).

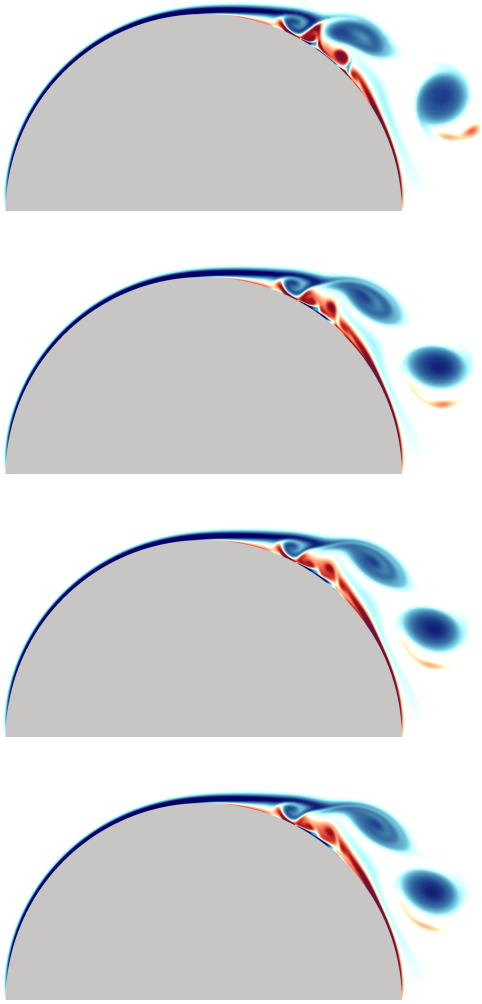

FIGURE 6. 2-D FLOW OVER IMPULSIVELY STARTED CYLINDER, $\mathrm{RE}_D = 9{,}500$, $T_R = 3$, EULERIAN MESH TO $1.05R$, VARYING VORTEX PARTICLE SIZE AND TIME STEP SIZE, $\Delta T_R = 0.02, 0.01, 0.005, 0.0025$ (TOP TO BOTTOM).

responding to nominal particle separation distances of $\{0.00251, 0.00178, 0.00126, 0.000889\}$. In all cases, the Eulerian regime uses 7×780 3rd-order quad cells, with $h \approx 0.004$, extending to $r/R = 1.05$, and twelve 4th-order Runge-Kutta substeps per outer time step (except for the lowest particle resolution, which required 25 substeps for stability). Each simulation was run to $t_R = 3$, with the vorticity field plotted on a grid of 2nd-order quads, and the Eulerian vorticity plotted over it using its original elements' geometry. These results appear in Fig. 6. Readily apparent is the convergence of the results as particle resolution increases: both the thin positive wisp (red) and the pair of positively-signed body-local discrete secondary vortices approach the high-order Eulerian $r/R = 1.5$ solution from Fig. 5.

Effects of other parameters Other parameter studies showed little effect on final results; those include: varying the number of iterations in the grid-to-particle overlap update, widening or moving the center of the overlap regions (within limits), varying the order of the substep time stepping (1 was poor, 2-4 were fine), varying the number of substeps in the Eulerian update step (as long as it was stable).

CONCLUSIONS

We have presented a two-dimensional, open-source, hybrid computational fluid dynamics tool for accurate simulation of un-

steady internal and external flows. The software includes a novel High-Order Eulerian scheme for near-body vorticity generation while retaining the LVPM for wake convection. The combination of high order Eulerian elements and the new hybrid scheme allows much thinner and less computationally-intense grid regions around wall boundaries. The method has demonstrated accuracy on both a lid-driven cavity and an impulsively-started cylinder flow compared to previous spectral and high-resolution results. Future work will refine the concepts herein and apply them to three-dimensional flows.

ACKNOWLEDGMENT

Research reported in this publication was supported by the National Institute Of Biomedical Imaging And Bioengineering of the National Institutes of Health under Award Number R01EB022180. The content is solely the responsibility of the authors and does not necessarily represent the official views of the National Institutes of Health.

REFERENCES

[1] Gharakhani, A., 2021. "A High-Order Flux Reconstruction Method For 2-D Vorticity Transport". In Proceedings of the ASME 2021 Fluids Engineering Division Summer Meeting, no. FEDSM2021-63196.

[2] Spalart, P. R., Leonard, A., and Baganoff, D., 1983. "Vortex Methods for Separated Flows". Tech. Rep. NASA TM-84328.

[3] Guermond, J.-L., Huberson, S., and Shen, W.-Z., 1993. "Simulation of 2d external viscous flows by means of a domain decomposition method". *J. Comput. Phys.,* ***108***(2), pp. 343–352.

[4] Cottet, G.-H., and Koumoutsakos, P., 1999. *Vortex Methods: Theory and Practice*. Cambridge Univ. Press, Cambridge, UK.

[5] Ould-Salihi, M. L., Cottet, G.-H., and Hamraoui, M. E., 2000. "Blending finite-difference and vortex methods for incompressible flow computations". *SIAM J. Sci. Comput.,* ***22***(5), pp. 1655–1674.

[6] Daeninck, G., 2006. "Developments in hybrid approaches: Vortex method with well known separation location, Vortex method with near-wall Eulerian solver, RANS-LES coupling". PhD thesis, Université catholique de Louvain.

[7] Stock, M. J., Stone, C. P., and Gharakhani, A., 2010. "Modeling Rotor Wakes with a Hybrid OVERFLOW-Vortex Method on a GPU Cluster". In 28th AIAA Applied Aerodynamics Conference, no. AIAA-2010-4553.

[8] Stone, C. P., Hennes, C., and Duque, E. P., 2010. "A Hybrid CPU/GPU Parallel Algorithm for Coupled Eulerian and Vortex Particle Methods". In Parallel Computational Fluid Dynamics: Recent Advances and Future Directions, R. Biswas, ed., pp. 251–262.

[9] Whitehouse, G. R., and Tadghighi, H., 2010. "Investigation of Hybrid Grid-Based Methods for Rotorcraft Flow Analysis". In American Helicopter Society Aeromechanics Specialists Meeting.

[10] Oxley, G. S., 2009. "A 2-D hybrid euler-compressible vortex particle method for transonic rotorcraft flows". PhD thesis, Carleton University.

[11] Papadakis, G., and Voutsinas, S. G., 2014. "In view of accelerating CFD simulations through coupling with vortex particle approximations". *J. Phys.: Conf. Ser.,* ***524***(012126).

[12] Palha, A., Manickathan, L., Ferreira, C. S., and van Bussel, G., 2015. "A hybrid Eulerian-Lagrangian flow solver". *arXiv preprint arXiv:1505.03368*.

[13] Spalart, P. R., 1988. "Vortex Methods for Separated Flows". Tech. Rep. NASA TM-100068.

[14] Gharakhani, A., 2007. "3-D Vortex Simulation Of Accelerating Flow Over A Simplified Opening Bileaflet Valve". In Proceedings of FEDSM2007 5th Joint ASME/JSME Fluids Engineering Conference, no. FEDSM2007-37134.

[15] Stock, M. J., and Gharakhani, A., 2011. "Graphics Processing Unit-Accelerated Boundary Element Method and Vortex Particle Method". *J. Aero. Comp. Inf. Com.,* ***8***(7), July, pp. 224–236.

[16] Stock, M. J., and Gharakhani, A., 2020. "Open-Source Accelerated Vortex Particle Methods for Unsteady Flow Simulation". In Proceedings of the ASME 2020 Fluids Engineering Division Summer Meeting, no. FEDSM2020-83730.

[17] Shankar, S., and van Dommelen, L., 1996. "A New Diffusion Procedure for Vortex Methods". *J. Comput. Phys.,* ***127***, pp. 88–109.

[18] Gharakhani, A., 2001. "Grid-Free Simulation of 3-D Vorticity Diffusion by a High-Order Vorticity Redistribution Method". In 15th AIAA Computational Fluid Dynamics Conference, no. AIAA-2001-2640.

[19] Huynh, H. T., 2007. "A Flux Reconstruction Approach to High-Order Schemes Including Discontinuous Galerkin Methods". In 18th AIAA Computational Fluid Dynamics Conference, no. AIAA-2007-4079.

[20] Huynh, H. T., 2009. "A Reconstruction Approach to High-Order Schemes Including Discontinuous Galerkin for Diffusion". In 47th AIAA Aerospace Sciences Meeting Including The New Horizons Forum and Aerospace Exposition, no. AIAA-2009-403.

[21] Geuzaine, C., and Remacle, J.-F., 2009. "Gmsh: A 3-D finite element mesh generator with built-in pre-and post-processing facilities". *Int. J. Numer. Methods Eng.,* ***79***(11), pp. 1309–1331.

[22] Koumoutsakos, P., Leonard, A., and Pepin, F., 1994. "Boundary conditions for viscous vortex methods". *J. Com-*

put. Phys., ***113***(1), pp. 52–61.
[23] Beale, J. T., 1988. "On the accuracy of vortex methods at large times". In *Computational Fluid Dynamics and Reacting Gas Flows*. Springer, pp. 19–32.
[24] Stock, M. J., and Gharakhani, A., 2020. "Omega2D: Two-Dimensional Flow Solver with GUI Using Vortex Particle and Boundary Element Methods". https://github.com/Applied-Scientific-Research/Omega2D.
[25] Vatistas, G. H., Kozel, V., and Mih, W., 1991. "A simpler model for concentrated vortices". *Exp. Fluids,* ***11***(1), pp. 73–76.
[26] Barnes, J. E., and Hut, P., 1986. "A Hierarchical O (N log N) Force Calculation Algorithm". *Nature,* ***324***, pp. 446–449.
[27] Greengard, L., and Rokhlin, V., 1987. "A Fast Algorithm for Particle Simulations". *J. Comput. Phys.,* ***73***, pp. 325–348.
[28] Demidov, D., 2019. "AMGCL: an efficient, flexible, and extensible algebraic multigrid implementation". *Lobachevskii J. Math.,* ***40***(5), May, pp. 535–546.
[29] Ghia, U., Ghia, K., and Shin, C., 1982. "High-Re Solutions for Incompressible Flow Using the Navier-Stokes Equations and a Multigrid Method". *J. Comput. Phys.,* ***48***, pp. 387–411.
[30] Erturk, E., Corke, T. C., and Gökçöl, C., 2005. "Numerical solutions of 2-D steady incompressible driven cavity flow at high Reynolds numbers". *Intl. J. Numer. Methods Fluids,* ***48***(7), pp. 747–774.
[31] Koumoutsakos, P., and Leonard, A., 1995. "High-resolution simulations of the flow around an impulsively started cylinder using vortex methods". *J. Fluid Mech.,* ***296***, pp. 1–357.
[32] Subramaniam, S., 1996. "A new mesh-free vortex method". PhD thesis, Florida State University.
[33] Kruse, G. W., 1997. "Parallel nonconforming spectral element methods". PhD thesis, Brown University.
[34] Wang, L., 2016. "High-performance discrete-vortex algorithms for unsteady viscous-fluid flows near moving boundaries". PhD thesis, University of California, Berkeley.
[35] Lee, S.-J., 2017. "Numerical simulation of vortex-Dominated flows using the penalized VIC method". In Vortex Dynamics and Optical Vortices, InTech, pp. 55–83.
[36] Chang, C.-C., and Chern, R.-L., 1991. "Vortex Shedding From an Impulsively Started Rotating and Translating Circular Cylinder". *J. Fluid Mech.,* ***233***, pp. 265–298.
[37] Rossinelli, D., Hejazialhosseini, B., van Rees, W., Gazzola, M., Bergdorf, M., and Koumoutsakos, P., 2015. "MRAG-I2D: Multi-resolution adapted grids for remeshed vortex methods on multicore architectures". *J. Comput. Phys.,* ***288***, pp. 1–18.